# Electrochemical Synthesis of Metal Phosphide under Mild Conditions: Mechanistic Insights and Application to Proton Reduction

Naoki Shida, Joshua A. Buss and Theodor Agapie*

Division of Chemistry and Chemical Engineering, California Institute of Technology, 1200 East California Boulevard, MC 127-72, Pasadena, California 91125, United States

**Supporting Information**

**Contents**

## *1. General Consideration*

Unless otherwise specified, all operations were carried out in an MBraun drybox under a nitrogen atmosphere or using standard Schlenk and vacuum line techniques. Solvents for air- and moisture-sensitive reactions were dried by the method of Grubbs.[1] $C_6D_6$ was purchased from Cambridge Isotope Laboratories and vacuum transferred from sodium benzophenone ketyl. Solvents, once dried and degassed, were stored under inert atmosphere over activated 4 Å molecular sieves. $Me_2NPA$,[2] ClPA,[2] $Mg(THF)_3(C_{14}H_{10})$,[3] and $Me_2NPCl_2$,[4] were prepared according to literature procedures. Unless indicated otherwise, all chemicals were used as received. $PCl_3$ (vacuum distilled from $CaH_2$), $HNMe_2$ (condensed trap-to-trap (0 °C to -78 °C)), HCl (4.0 M in dioxane), $Ni(COD)_2$ (COD = 1,5-cyclooctadiene), and sulfuric acid (99.999%) were purchased from Sigma Aldrich. $NiCl_2$(DME) (DME = 1,2-dimethoxyethylene) was purchased from Strem. Anthracene was bought from Acros Organics. Titanium foil (0.25 mm thick, 99.5%) was purchased from Alfa Aesar. The Pt wire electrode (φ = 0.5 mm, 32 mm in length) was purchased from CH Instruments. The graphite rod was purchased from Ted Pella, Inc. $^1H$, $^{13}C\{^1H\}$, and $^{31}P\{^1H\}$ NMR spectra were recorded on a Varian 400 MHz or Varian INOVA-500 spectrometers with shifts reported in parts per million (ppm). $^1H$ and $^{13}C\{^1H\}$ NMR spectra are referenced to residual solvent peaks.[5] $^{31}P\{^1H\}$ chemical shifts are referenced to an external 85% $H_3PO_4$ (0 ppm) standard. Multiplicities are abbreviated as follows: s = singlet, d = doublet, dd = doublet of doublets, dt = doublet of triplets, t = triplet, m = multiplet, and br = broad. Elemental analysis was performed at the Caltech XRCF using a PerkinElmer 2400 Series II CHN Elemental Analyzer. Powder X-ray diffraction (PXRD) was performed at Caltech Applied Material Physics and Material Science division using PANalytical X'Pert Pro. For the data analysis, PANalytical X'Pert High Score software was used. Scanning electron microscope (SEM) observation and Energy-dispersive X-ray spectroscopy (EDX) analysis were performed at Caltech Geological and Planetary Sciences Division using Zeiss 1550VP field emission SEM equipped with Oxford EDX. For SEM, the SmartSEM software package was used, and all measurements were performed with 10-kV accelerating potential with an SE2 detector. EDX measurements and data analysis were performed using AZtec software. X-ray photoelectron spectroscopy (XPS) data were collected at Beckman Institute in Caltech using a Surface Science Instruments M-Probe ESCA controlled by Hawk Data Collection software (Service Physics, Bend OR; V7.04.04).

## *2. Synthesis*

Synthesis of **1**

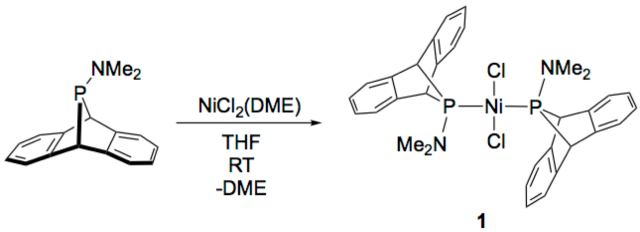


**1**

To a THF suspension of $NiCl_2$(DME) (43.9 mg, 0.2 mmol), $Me_2NPA$ (0.4 mmol) in THF was added dropwise. The pale yellow mixture immediately turned red. After removal of the volatiles *in vacuo*, the remaining solids were dissolved in minimal THF (ca. 5 mL),

filtered, and layered with pentane (10 mL). The layered solution placed in a -35 °C freezer. Red crystalline blocks of **1** were obtained after one week. The solvent was removed via decantation; the red crystals were then washed with pentane, dried *in vacuo*, and collected as analytically pure **1** (78.9 mg, 0.124 mmol, 62%).

$^{1}$H NMR (500 MHz, $C_6D_6$, 10 °C) δ: 7.54 (dd, *J* = 5.5, 3.2 Hz, 4H, Aryl-*H*), 7.08 (dd, *J* = 5.6, 3.2 Hz, 4H, Aryl-*H*), 6.97 (dd, *J* = 5.4, 3.2 Hz, 4H, Aryl-*H*), 6.76 (dd, *J* = 5.4, 3.1 Hz, 4H, Aryl-*H*), 4.85 (s, 4H, bridgehead-*H*), 2.33 (t, *J* = 4.1 Hz, 12H, N(C*H*$_3$)$_2$). $^{13}$C{$^{1}$H} NMR (126 MHz, $C_6D_6$, 10 °C) δ: 144.14 (s, Aryl-*C*), 141.18 (t, *J* = 10.1 Hz, Aryl-*C*), 126.82 (s, Aryl-*C*), 126.15 (s, Aryl-*C*), 125.38 (s, Aryl-*C*), 123.31 (s, Aryl-*C*), 52.65 (s, bridgehead-*C*), 41.45 (s, N(*C*H$_3$)$_2$). $^{31}$P{$^{1}$H} NMR (202 MHz, $C_6D_6$, 10 °C) δ: 160.74 (s).

Synthesis of **2**

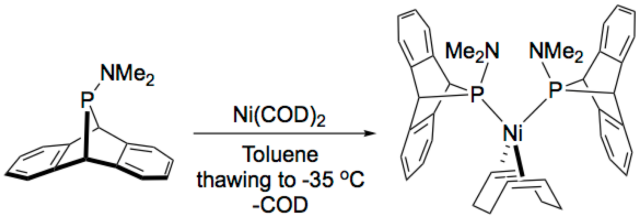


**2**

A 20 mL scintillation vial charged with toluene solution (5 mL) of Ni(COD)$_2$ (110 mg, 0.4 mmol) was frozen in a $LN_2$-cooled cold well. Immediately upon thawing, a thawing solution of **Me$_2$NPA** (0.8 mmol) in toluene (5 mL) was added dropwise, mixed at low temperature, and the vial contents refrozen. Atop the frozen reaction mixture, a layer of thawing pentane (10 mL) was added. The vial was sealed, and allowed to warm to -35 °C in the glove box freezer. Green crystalline blocks of **2** were obtained after one week. The solvent was removed by decantation; the remaining crystals were washed with pentane, dried *in vacuo*, and collected as analytically pure **2** (196.5 mg, 0.279 mmol, 70%).

$^{1}$H NMR (500 MHz, $C_6D_6$, 10 °C) δ: 7.21 (dd, *J* = 5.4, 3.2 Hz, 4H, Aryl-*H*), 7.18 (dd, *J* = 5.3, 3.1 Hz, 4H, Aryl-*H*), 6.94 (dt, *J* = 5.8, 2.9 Hz, 8H, Aryl-*H*), 4.29 (d, *J* = 6.1 Hz, 4H, bridgehead-*H*), 3.68 (d, *J* = 11.0 Hz, 4H, -C*H*- of COD), 2.15 (br, 8H, -C*H*$_2$- of COD), 2.12 (d, *J* = 7.5 Hz, 2H, N(C*H*$_3$)$_2$). $^{13}$C{$^{1}$H} NMR (126 MHz, $C_6D_6$, 10 °C) δ: 147.78 (s, Aryl-*C*), 144.82 (d, *J* = 18.6 Hz, Aryl-*C*), 126.12 (s, Aryl-*C*), 125.05 (s, Aryl-*C*), 124.56 (s, Aryl-*C*), 123.30 (s, Aryl-*C*), 84.01 (s, -*C*H- of COD), 57.78 (s, bridgehead-*C*), 40.30 (s, N(*C*H$_3$)$_2$), 31.80 (s, -*C*H- of COD). $^{31}$P{$^{1}$H} NMR (202 MHz, $C_6D_6$, 10 °C) δ: 235.5.

Synthesis of **3**

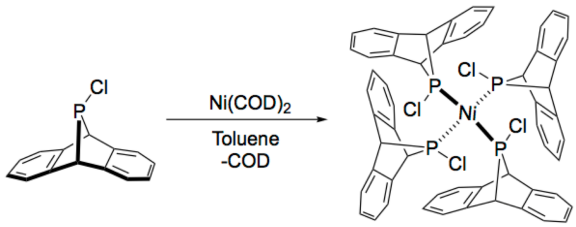


**3**

*Method 1* – To a thawing toluene (2 mL) solution of $Ni(COD)_2$ (27.5 mg, 0.1 mmol) in a 1 dram vial, thawing **ClPA** (0.1 mmol) in toluene (1 mL) was added. The resulting solution was mixed at low temperature and refrozen. The dram vial was placed inside a pre-chilled 20 mL vial and thawing pentane was transferred to the interstitial space. The entire contents of the 20 mL vial were frozen solid and the vial capped. It was then placed in the glove box freezer and slowly warmed to -35 $^{o}$C. Slow vapor diffusion afforded yellow-green single crystals of **3**. The solvent was removed by decantation, and the crystals washed with pentane, affording analytically pure **3** (yield not recorded, see method 2 for yield).

*Method 2* – A 20 mL scintillation vial was charged with a THF solution (10 mL) of **ClPA** (1.6 mmol) and a stir bar. With stirring, $Ni(COD)_2$ (110 mg, 0.4 mmol) in THF (5 mL) was added dropwise, at room temperature, maintaining a high **ClPA** concentration relative to $Ni(COD)_2$. During the addition, the solution color turned green. After stirring for 1 h, the solvent was evaporated under reduced pressure. The resulting solids were washed with $Et_2O$ (ca. 60 mL). The remaining yellow-green residue was dissolved in THF (ca. 10 mL), and layered with pentane (ca. 10 mL). The vial was sealed and placed in a -35 $^{o}$C freezer in the glove box. Green crystals were obtained after one week. Decantation of the solvent, washing of the remaining crystals with pentane, and removal of volatiles *in vacuo* afforded analytically pure **3** (148 mg, 0.142 mmol, 36%) as green crystalline blocks.

$^{1}$H NMR (500 MHz, $C_6D_6$, 10 °C) δ: 7.26 (dd, $J$ = 5.4, 3.2 Hz, 8H, Aryl-*H*), 7.14 (dd, $J$ = 5.3, 3.2 Hz, 8H, Aryl-*H*), 7.01 (dd, $J$ = 5.5, 3.2 Hz, 8H, Aryl-*H*), 6.90 (dd, $J$ = 5.3, 3.1 Hz, 8H, Aryl-*H*), 4.05 (s, 1H, bridgehead-*H*). $^{13}$C{$^{1}$H} NMR (126 MHz, $C_6D_6$, 10 °C) δ: 146.35 (s, Aryl-*C*), 141.13 (br m, Aryl-*C*), 127.13 (s, Aryl-*C*), 126.56 (s, Aryl-*C*), 125.42 (s, Aryl-*C*), 124.02 (s, Aryl-*C*), 61.02 (s, bridgehead-*C*). $^{31}$P{$^{1}$H} NMR (202 MHz, $C_6D_6$, 10 °C) δ: 213.92.

## 3. *NMR spectra*

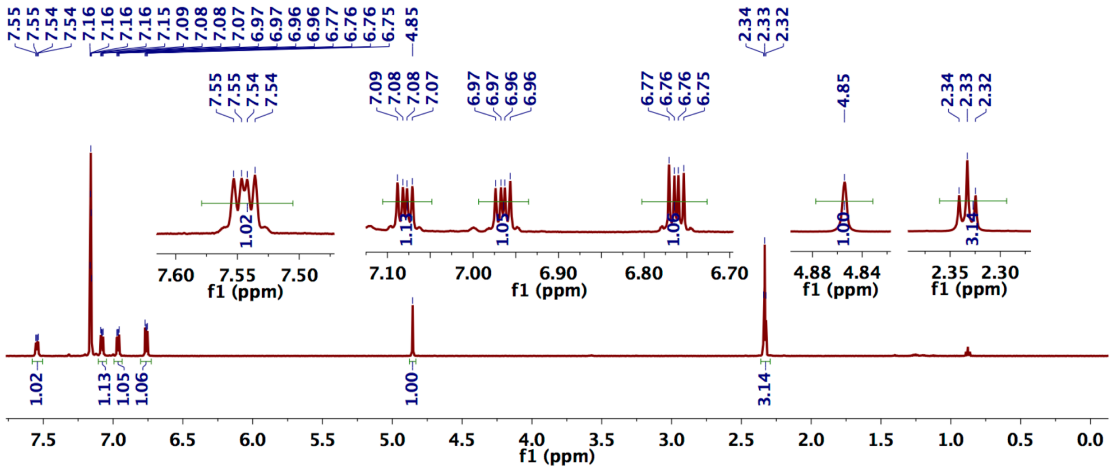

**Fig. S1** $^{1}$H NMR spectrum (500 MHz, $C_6D_6$, 10 °C) of **1**.

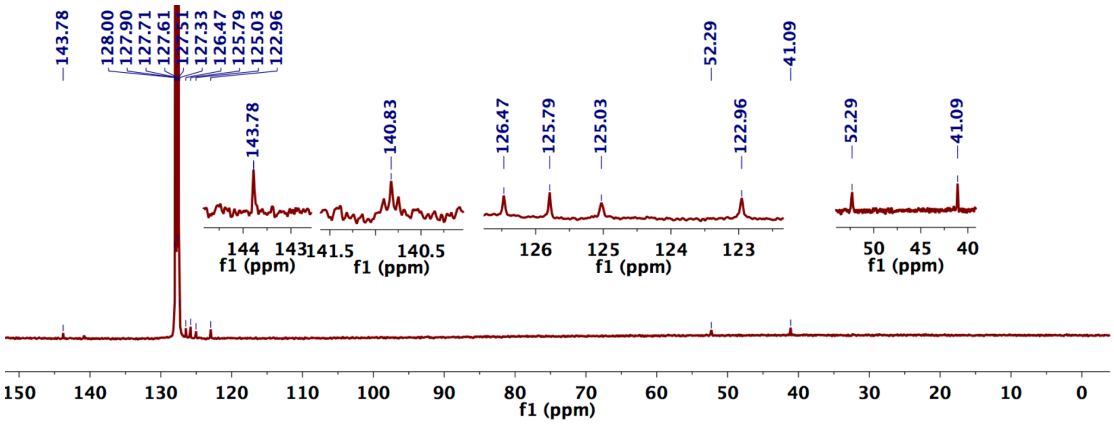

**Fig. S2** $^{13}$C NMR spectrum (126 MHz, $C_6D_6$, 10 °C) of **1**.

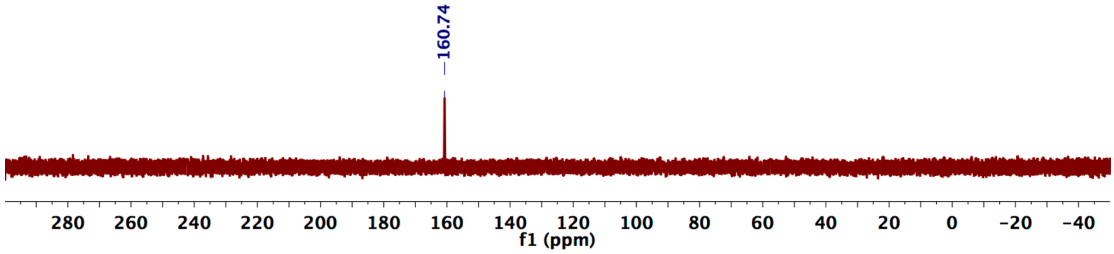

**Fig. S3** $^{31}$P NMR spectrum (202 MHz, $C_6D_6$, 10 °C) of **1**.

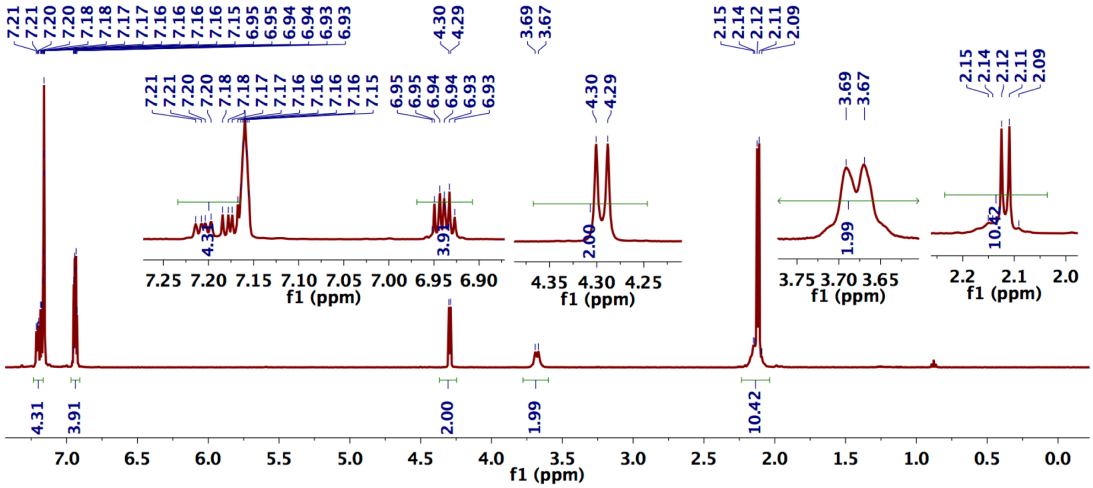

**Fig. S4** $^{1}$H NMR spectrum (500 MHz, $C_6D_6$, 10 $^{o}$C) of **2**.

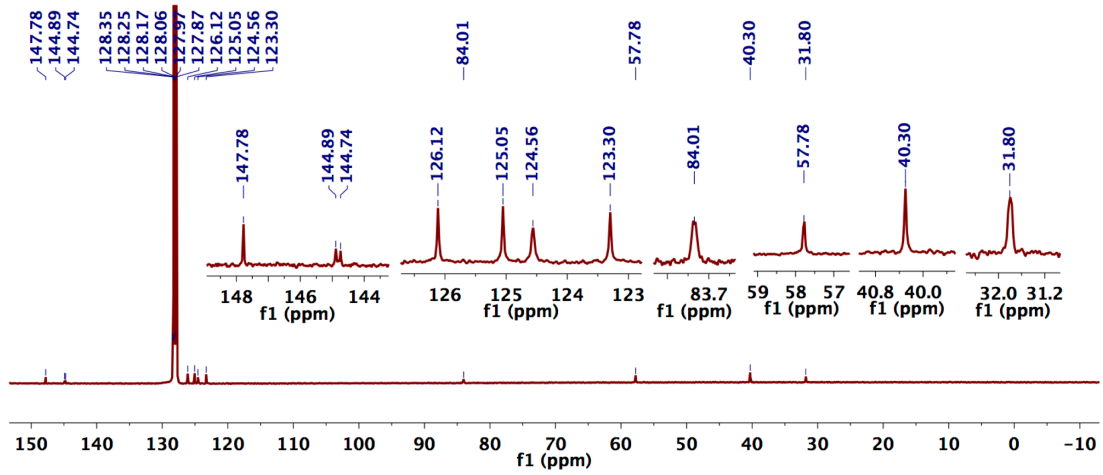

**Fig. S5** $^{13}$C NMR spectrum (126 MHz, $C_6D_6$, 10 $^{o}$C) of **2**.

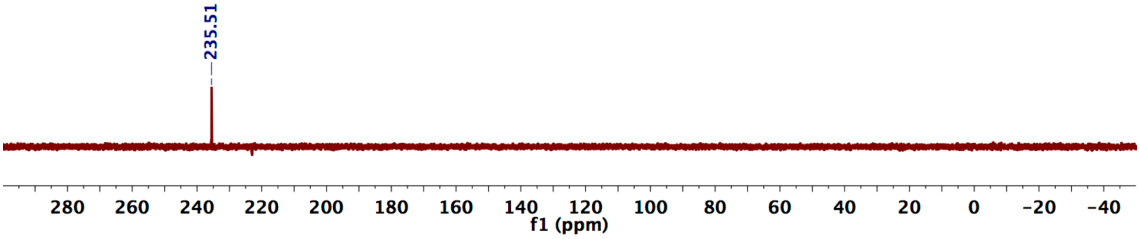

**Fig. S6** $^{31}$P NMR spectrum (202 MHz, $C_6D_6$, 10 $^{o}$C) of **2**.

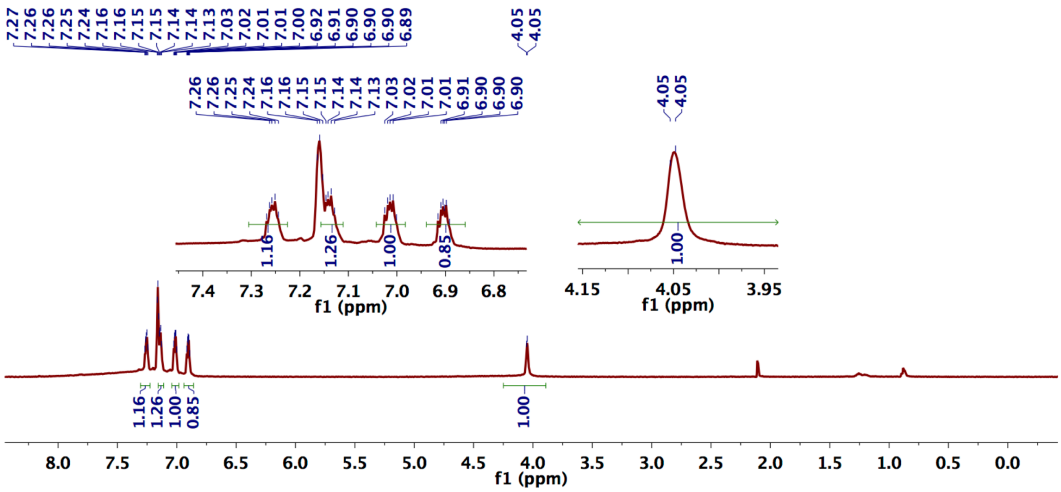

**Fig. S7** $^{1}$H NMR spectrum (500 MHz, $C_6D_6$, 10 °C) of **3**.

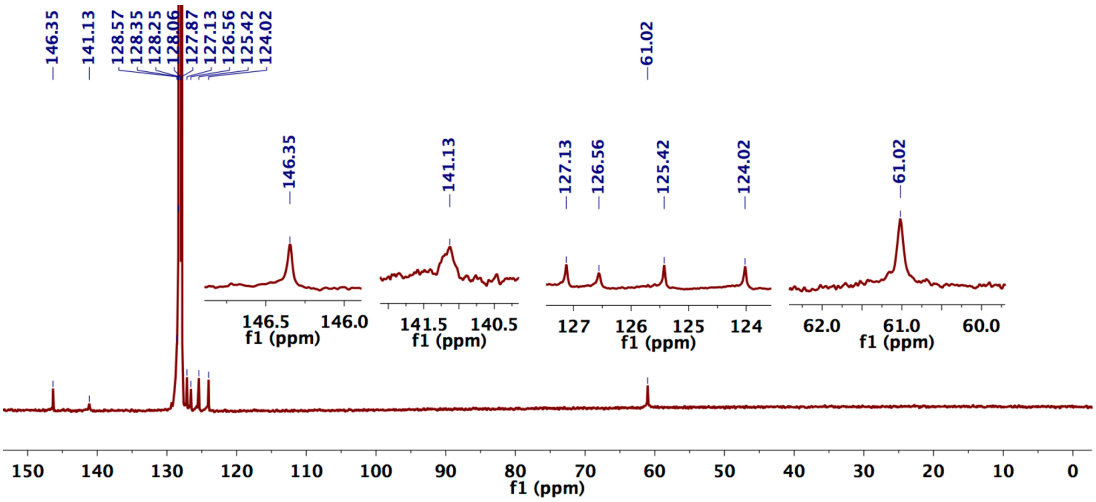

**Fig. S8** $^{13}$C NMR spectrum (126 MHz, $C_6D_6$, 10 °C) of **3**.

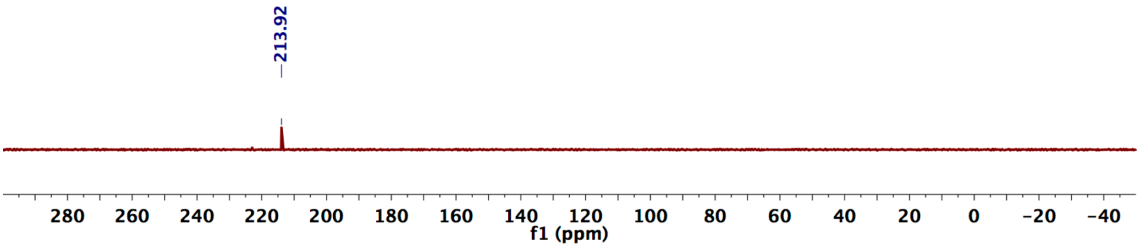

**Fig. S9** $^{31}$P NMR spectrum (202 MHz, $C_6D_6$, 10 °C) of **3**.

## 4. *Characterization of precipitate obtained from the room temperature reaction of ClPA with $Ni(COD)_2$*

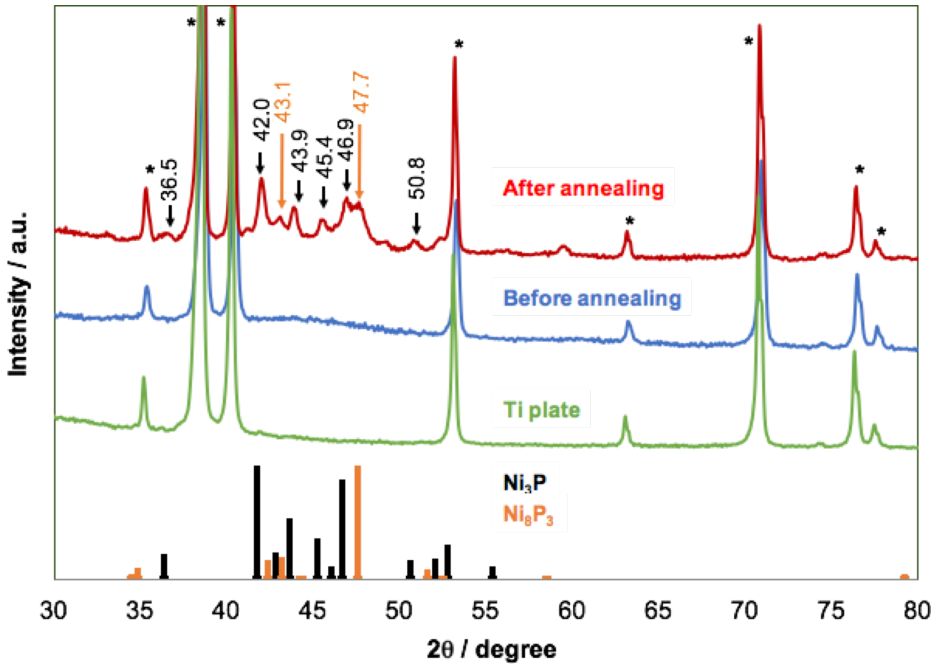


**Fig. S10** PXRD pattern of precipitate obtained from the reaction of $Ni(COD)_2$ and 2 eq. of **ClPA**, before (blue) and after (red) annealing at 450 °C under a 5% $H_2$/balance $N_2$ gas flow (2 L/min). PXRD patterns of Ti plate (green), $Ni_3P$ (black) and $Ni_8P_3$ (orange) are included for reference.[6]

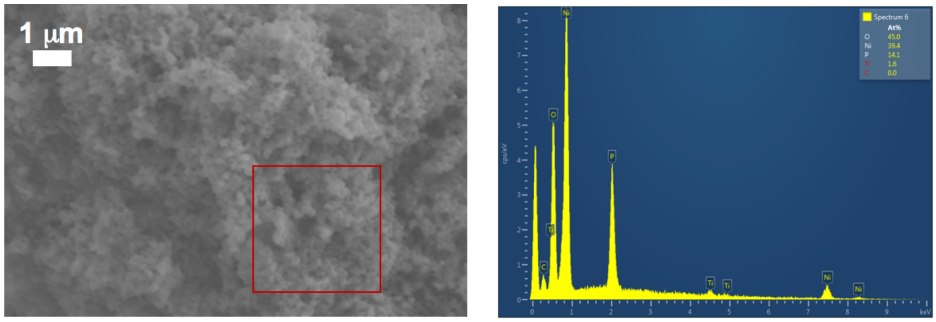


**Fig. S11** SEM image and EDX elemental analysis of the precipitate before annealing.

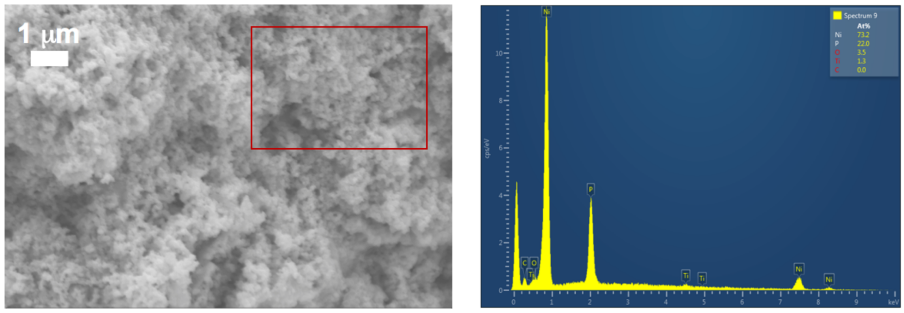


**Fig. S12** SEM image and EDX elemental analysis of the precipitate after annealing.

## 5. *Thermal stability of 1-3*

The thermal stabilities of complexes **1-3** were examined at 25 °C and 40 °C by $^1$H NMR spectroscopy. **1-3** were dissolved in $C_6D_6$ (0.7 mL) with a 1,3,5-trimethoxybenzene (2.0 mg, 0.012 mmol) internal standard, then loaded into a J-Young style NMR tube. Fig. S13a shows the downfield region of partial $^1$H NMR spectra of **1-3**. Peaks denoted with asterisks were integrated as representative resonances of **1-3**, and the molar ratio calculated with respect to the internal standard. For the molar ratio calculations of free anthracene and COD, resonances at 8.17 and 5.56 ppm were selected, respectively.

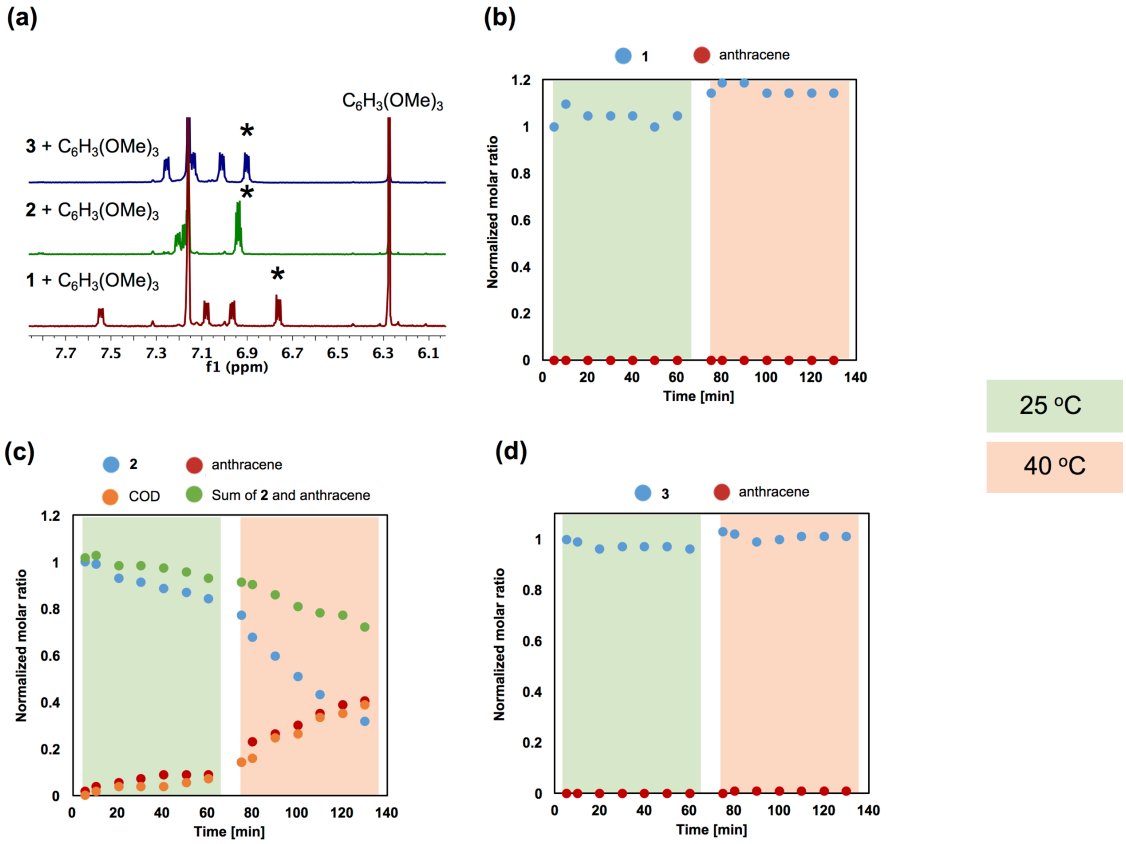


**Fig. S13** (a) Partial $^1$H NMR spectra of **1-3** with a $C_6H_3(OMe)_3$ internal standard. The asterisk indicates the peak selected for integration. (b-d) Normalized molar ratios of the species of interest as a function of time.

### *6. CV measurement using Ni-P modified GC disc electrode*

Electrochemical behavior of Ni-P was investigated by CV measurement. After 50 deposition cycle, film formation was observed as shown in Fig. S14a. The modified electrode was washed with THF. The electrode was then set in 0.1 M $^{n}Bu_4NPF_6$/THF and CV measurements were performed (Fig. S14b, yellow trace). Ni-P modified GC showed larger non-Faradaic current, presumably due to the increase of electroactive surface area. Compared to the CV recorded in the course of the deposition (Fig. S14b, red trace), anodic current around -0.25 V and cathodic current around -0.9 V of the Ni-P decreased, indicating these derived from the redox of Ni(II) species in solution. The CV of Ni-P modified electrode recorded in 5 mM ClPA solution (Fig. S14b, green trace) showed identical voltammogram to the one recorded in blank solution. Additionally, the peak current of the film was proportional to the scan rate (Fig. S14c, d). These results suggested that even after the deposition, ClPA is not involved in electrochemical redox process.

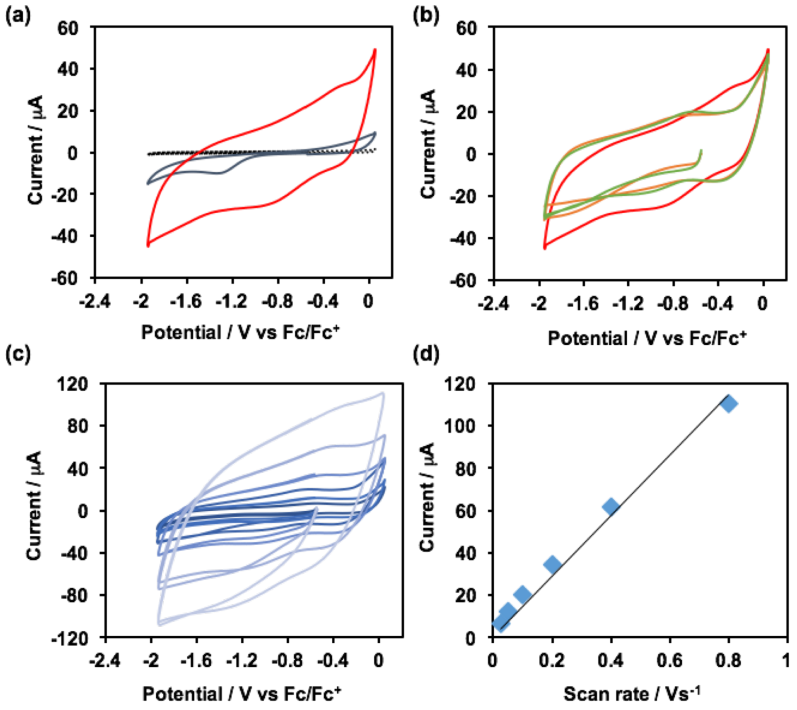


**Fig. S14** (a-c) CVs recorded in 0.1 M $^{n}Bu_4NPF_6$ in THF. (a) 1$^{st}$ (blue) and 50$^{th}$ (red) cycle of electrodeposition in 2.5 mM $NiCl_2$(DME) + 5 mM ClPA at a scan rate of 100 mV/s. (dot) CV recorded in 5 mM ClPA at a scan rate of 100 mV/s. (b) CV of Ni-P modified GC (50 cycle deposition) electrode in the absence (yellow) or the presence (green) of 5 mM ClPA. Red trace is the CV shown also in (a), for comparison. (c) CV of Ni-P modified GC (50 cycle deposition) in 5 mM ClPA solution at scan rate of 25, 50, 100, 200, 400 and 800 mV/s. (d) Plot of scan rate vs anodic peak current from CVs in (c).

## 7. *Effect of stoichiometry of ClPA in electrodeposition*

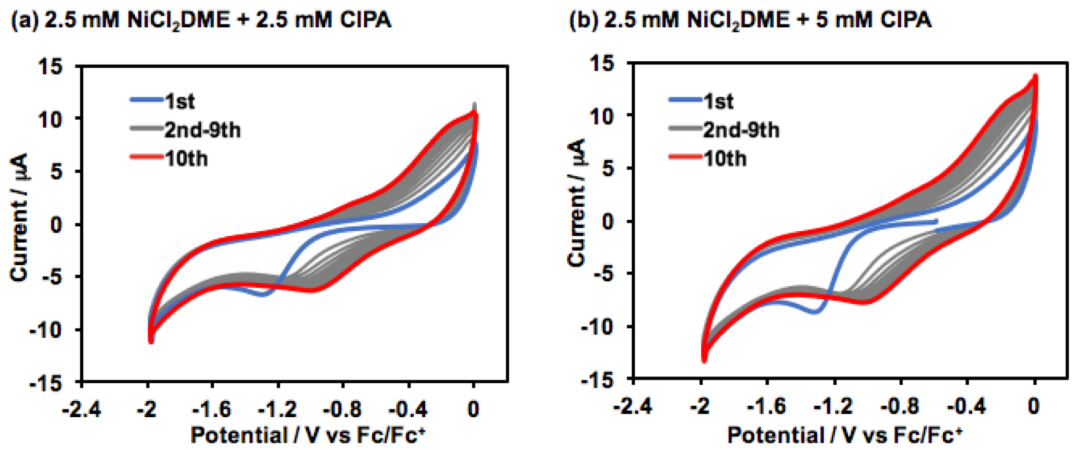


**Fig. S15** CVs of 2.5 mM $NiCl_2$DME and (a) 2.5 mM or (b) 5 mM of **ClPA** in 0.1 M $^nBu_4NPF_6$/THF with a scan rate of 100 mV/s, using a glassy carbon disc working electrode, a graphite rod counter electrode, and a silver wire reference electrode. Potentials were referenced to the ferrocene/ferrocenium redox couple.

## 8. *Electrochemistry of $PCl_3$*

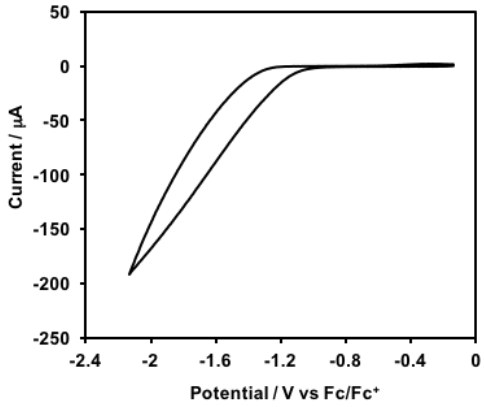


**Fig. S16** CV of 2.5 mM $PCl_3$ in 0.1 M $^nBu_4NPF_6$/THF with a scan rate of 100 mV/s, using a glassy carbon disc working electrode, a graphite rod counter electrode, and a silver wire reference electrode. Potentials were referenced to the ferrocene/ferrocenium redox couple.

### *9. Electrode Fabrication*

Working electrodes for bulk electrolysis were fabricated in the lab according to a procedure reported previously.[7] Ti foil was cut into pieces (5 mm x 5 mm) and attached to copper wire with silver paint (SPI supplies). The copper wire was then passed through glass tubes, and the entire back side of the Ti foil was covered with epoxy (Loctite Hysol 1C).

### *10. Cyclic Voltammogram Measurement and Bulk Electrosynthesis*

Cyclic Voltammogram (CV) measurements and bulk electrolyses to prepare M-P films were performed with a Pine Instrument Company AFCBP1 bipotentiostat using the AfterMath software package in a nitrogen filled glove box.

The CVs in Fig. 3 (main text) were recorded in a 0.1 M $^{n}Bu_4NPF_6$ electrolyte solution in THF. A Ag wire reference electrode, a graphite rod counter electrode and a glassy carbon disk working electrode ($\varphi$ = 3 mm) were employed in a single-compartment cell with a scan rate of 100 mV/s. Reported potentials were referenced internally to the redox couple of ferrocene (Fc) or decamethylferrocene, and are reported versus $Fc/Fc^+$.

Bulk electrolyses were performed in a 0.1 M $^{n}Bu_4NPF_6$ electrolyte solution in THF containing the appropriate metal source and ClPA (Table S1). A Ag wire reference electrode, a graphite rod counter electrode and a titanium foil working electrode (0.25 $cm^2$) were employed for each bulk electrolysis in a single-compartment cell. A potential of -1.7 V (vs $Fc/Fc^+$) was applied to the working electrode, and the electrolysis was continued for 1 h, with stirring. After the electrolysis, working electrodes were carefully washed with THF and dried in the glovebox.

**Table S1.** Conditions for bulk electrolysis

| | Metal source | Con. of metal source [mM] | Con. of ClPA [mM] |
|---|---|---|---|
| Ni-P | $NiBr_2$(DME) | 25 | 25 |
| Co-P | $CoI_2$ | 25 | 25 |
| Fe-P | $FeI_2$ | 10 | 10 |

### *11. Estimation of Faradaic Efficiency for electrodeposition*

Faradaic efficiency for electrodeposition of Ni-P was estimated by the following method. Titanium foil (2 cm x 1 cm) used as a working electrode was weighed on autobalance (AD6000, PerkinElmer) before the electrolysis. Titanium foil was connected to potentiostat by alligator clip. Graphite rod and silver wire were used as counter and reference electrode, respectively. 0.1 M $^{n}Bu_4NPF_6$/THF solution containing 25 mM $NiBr_2$DME and 25 mM ClPA was used as electrolyte. A potential of -1.7 V (vs $Fc/Fc^{+}$) was applied to the working electrode, and the electrolysis was continued for 1 h, with stirring. Current profile during the electrolysis is shown in Fig. S17. The amount of charge passed was -1.820 C. After the electrolysis, working electrode was carefully washed with THF and dried under vacuo in the glovebox. Ni-P modified Ti foil was weighed again in glove box. The increase in weight was 0.35 mg. EDX analysis Ni:P ratio of the film was close to 3:1 (Fig. S18). Assuming the deposition proceeds via a 7-electron reduction process based on the following equation, Faradaic efficiency for electrodeposition was 63%.

$$3NiBr_2 + ClPA + 7e^- \longrightarrow Ni_3P + 6Br^- + Cl^- + C_{14}H_{10}$$

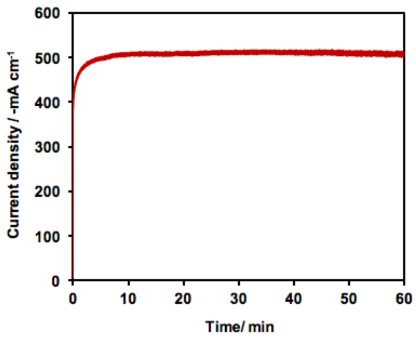


**Fig. S17** Time course of current density during constant-potential electrodeposition

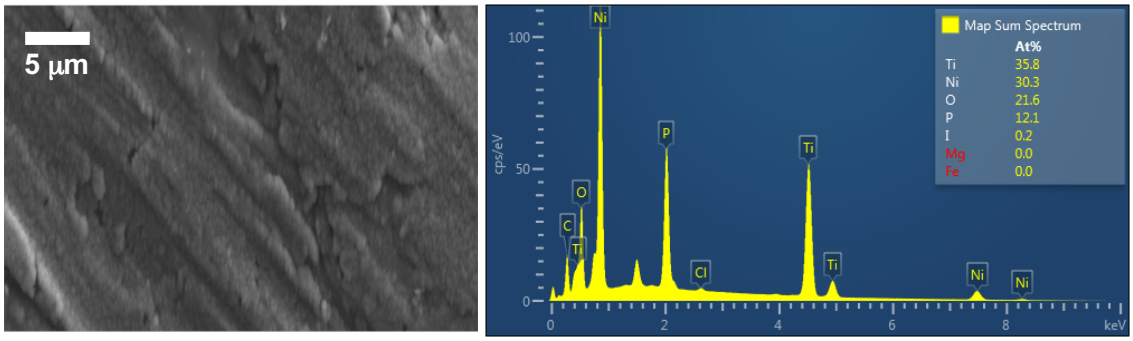


**Fig. S18** SEM image and EDX profile of obtained film

### *12.* $C_{10}H_{14}$ Quantification Following Electrodeposition

Electrolysis was conducted under identical conditions to those described in section 11. The amount of charge passed was -2.212 C. Based on the assumption that passing $7e^-$ releases 1 eq. of $C_{14}H_{10}$ (see section 11), the theoretical amount of $C_{14}H_{10}$ was calculated as follows:

$$Number\ of\ electron\ passed\ [mmol] = \frac{Charge\ passed\ [mC]}{Faraday\ constant\ [mC/mmol]}$$

$$= \frac{2.212 \times 10^3}{96485} = 0.02293\ mmol$$

$$C_{10}H_{14theo}\ [mmol]: \frac{0.02293\ mmol}{7} = 0.0033\ mmol$$

After the electrolysis, the electrodes were removed, and the volatile materials were removed *in vacuo*. The solid left in the vial was extracted with toluene (*ca.* 10 mL) and filtered through celite. The filtrate was brought to constant mass under reduced pressure to give orange-red solids. $C_6H_3(OMe)_3$ (11.6 mg, 0.069 mmol) was added as an internal standard. 2 mL of $C_6D_6$ was added to the vial, stirred vigorously, and the soluble part was analyzed by multinuclear NMR spectroscopy (Fig. S19, 20). The $^{31}P$ NMR spectrum showed two broad peaks and a single sharp resonance; the signals at 177.4 and 86.7 ppm correspond to free ClPA and an unidentified decomposition product of ClPA, respectively. From the relative integration of the $C_{10}H_{14}$ and $C_6H_3(OMe)_3$ resonances in the $^1H$ NMR spectrum, the amount of free $C_{14}H_{10}$ was calculated to be 0.010 mmol. The larger amount of anthracene compared to the theoretical amount based on electrochemistry is likely due to partial decomposition of ClPA through unproductive pathways (observed by $^{31}P$ NMR spectroscopy). However, considering that the total amount of ClPA in solution (25 mM, 5 mL: 0.125 mmol) is significantly higher, this minor decomposition pathway is not expected to hinder the formation of a Ni-P film.

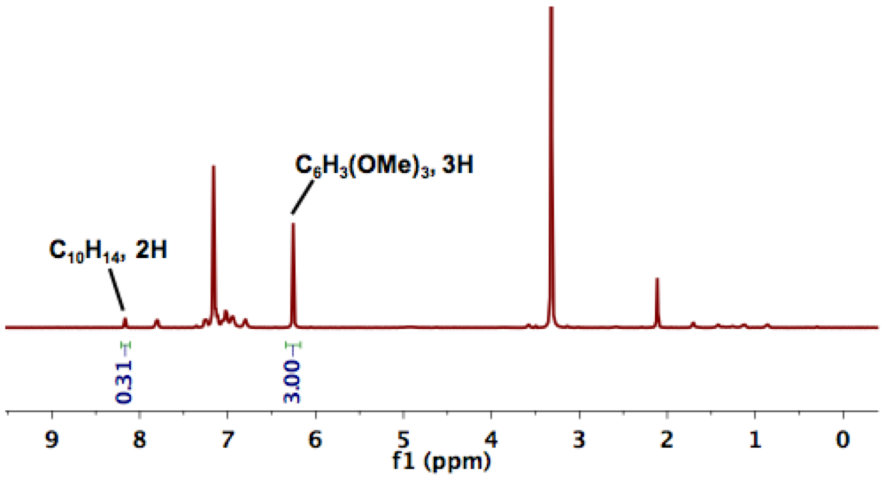


**Fig. S19** $^1H$ NMR spectrum (400 MHz, 21 °C, $C_6D_6$) of the toluene extract of the electrolyte solution

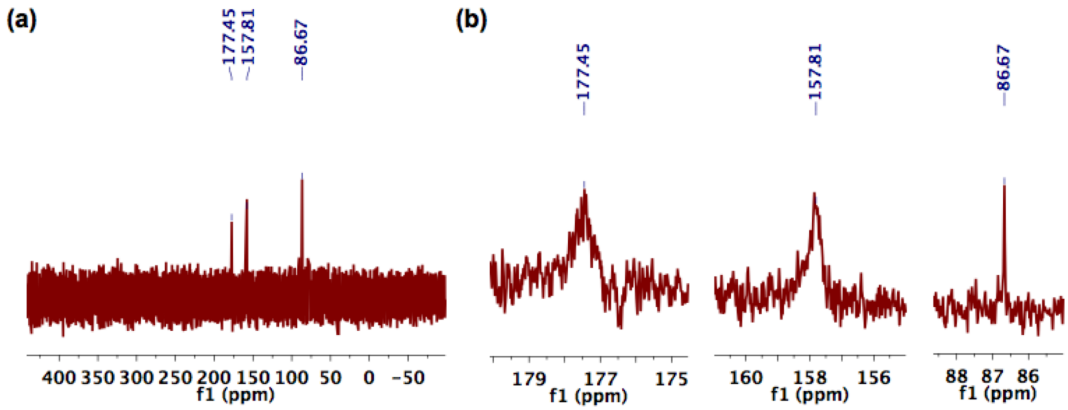


**Fig. S20** $^{31}$P NMR spectrum (162 MHz, 21 °C, $C_6D_6$) of the toluene extract of the electrolyte solution. Both the full spectrum (a) and enlargements of the observed resonances (b) are shown.

*13. SEM/EDX analysis on Ni-P, Co-P, and Fe-P film*

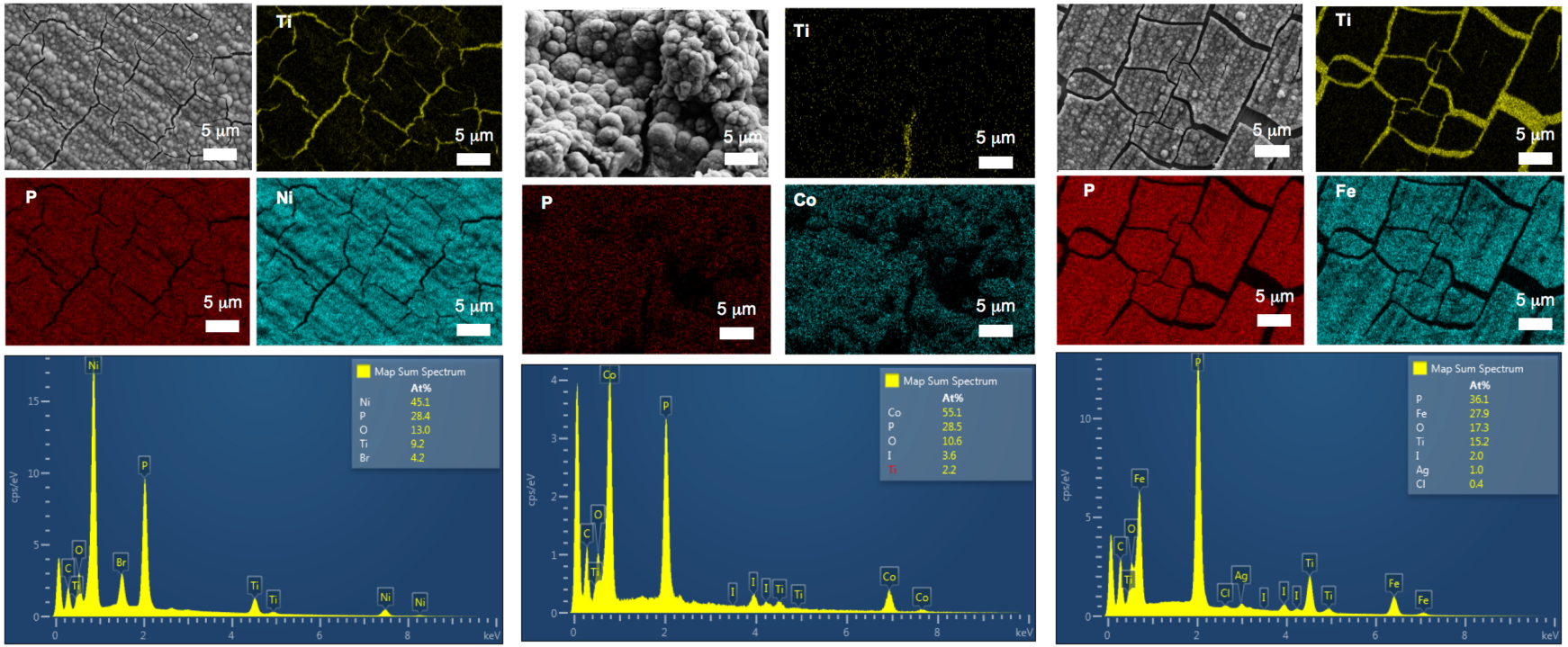


**Fig. S21** SEM image, elemental mapping and elemental analysis of Ni-P (left), Co-P (middle) and Fe-P (right)

*14. Side view of M-P film*

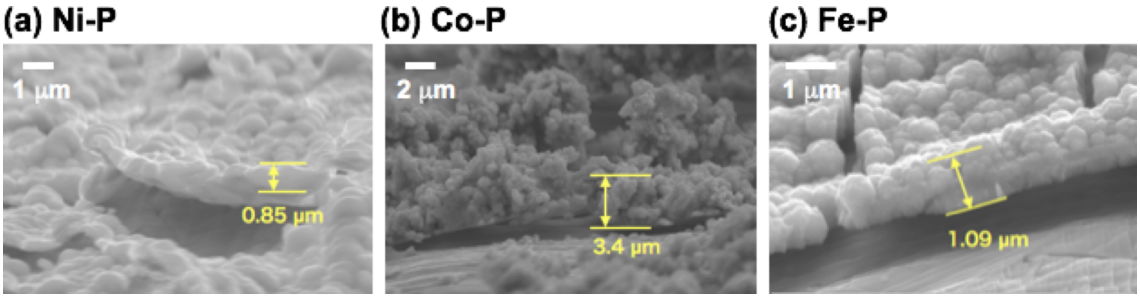


**Fig. S22** Side view of Ni-P, Co-P and Fe-P film (fabricated under the conditions shown in Table S1). Film thickness was estimated from the thickness of the flake of the film on the electrode.

### *15. XPS analysis on Ni-P, Co-P, and Fe-P film*

X-ray photoelectron spectroscopy (XPS) data were collected using a Surface Science Instruments M-Probe ESCA controlled by Hawk Data Collection software (Service Physics, Bend OR; V7.04.04). The monochromatic X-ray source was the Al $K_\alpha$ line at 1486.6 eV, directed at 35° to the sample surface (55° off normal). Emitted photoelectrons were collected at an angle of 35° with respect to the sample surface (55° off normal) by a hemispherical analyzer. The angle between the electron collection lens and X-ray source is 71°. Low-resolution survey spectra were acquired between binding energies of 1-1000 eV. Higher-resolution detailed scans, with a resolution of ~0.8 eV, were collected on individual XPS lines of interest. The sample chamber was maintained at $< 2 \times 10^{-9}$ Torr. The XPS data were analyzed using the CasaXPS software. In survey spectra, a pair of small peaks around 370 eV were detected, corresponding to Ag $3d_{3/2}$ and $3d_{5/2}$. This was attributed to the dissolution of the Ag reference electrode and subsequent deposition onto the working electrode. However, considering the detected amount of Ag was quite low in both XPS and EDX analysis, and the low catalytic activity of Ag (or NiAg alloy) for HER in comparison to metal phosphides,[8] we concluded that the effect of Ag was negligible. Additionally, Ni-P film prepared in the absence of Ag wire by constant-current electrolysis showed almost identical activity compared to the one prepared under constant-potential electrolysis (see section 17). This result also indicates that Ag is not responsible for HER activity in this system.

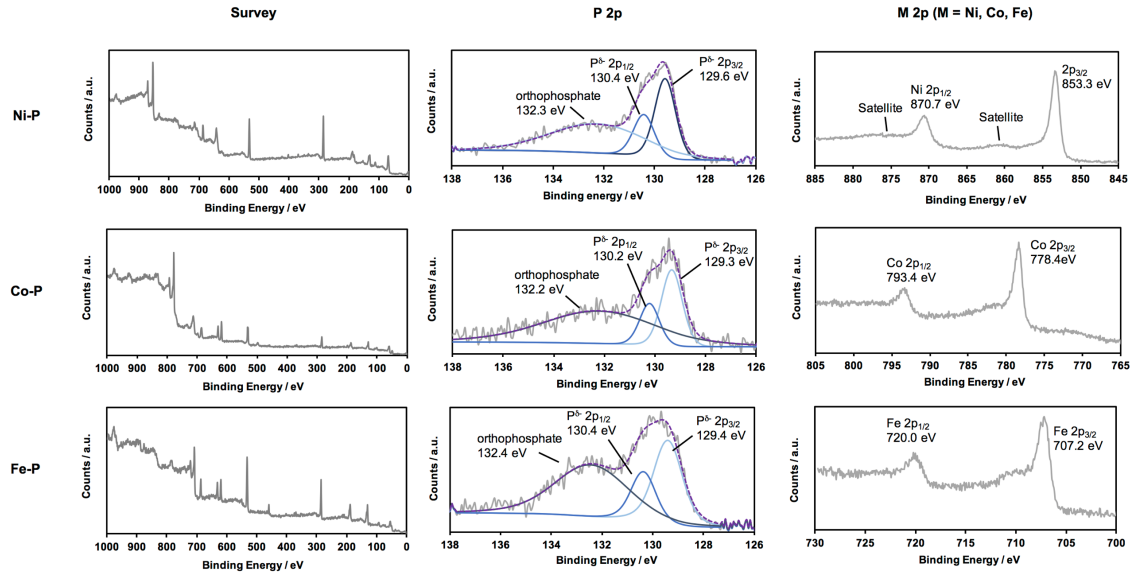


**Fig. S23** XPS of Ni-P, Co-P and Fe-P films. Survey spectra and high-resolution spectra at the P 2p and M 2p (M = Ni, Co, Fe) regions are shown.

### *16. Hydrogen Evolution Catalysis Measurement*

A Biologic VMP3 multichannel potentiostat was used for hydrogen evolution catalysis measurements. The experiments were conducted in a fume hood. A three electrode cell comprised of a working electrode, a graphite rod counter electrode and a Ag/AgCl (1 M KCl) reference electrode was emplolyed. 0.5 M $H_2SO_4$ was used as the electrolyte and the solution was satulated with research-grade $H_2$ by bubbling for 15 min prior to electrochemical measurements. The Ag/AgCl (1 M KCl) reference electrode was scaled to a reversible hydrogen electrode (RHE) reference based on the open-curcuit potential of a Pt wire working electrode in 0.5 M $H_2SO_{4(aq)}$ solution saturated with bubbling $H_2$. All the polarization data shown in Fig. 4e were recorded with a scan rate of 3 mV/s while rapidly stirring the solution with a magnetic stir bar and bubbling $H_2$. The measurements were conducted in both forward and reverse direction, and reverse scans are shown in Fig. 4a. All the data were IR-corrected based on the ohmic resistance estimated from electrochemical impedance measurements.[9] Reference HER data for a Pt wire working electrode was collected following electropolishing of the electrode surface.

### *17. Comparison catalytic activity of Ni-P film prepared by CPE and CCE*

To investigate the effect of preparation method of Ni-P in catalytic activity, two distinct Ni-P film was prepared by constant-potential electrolysis (CPE) and constant-current electrolysis (CCE). Experimental contdition for CPE is descrived in section 9. For CCE, current of 500 μA was passed for 60 min under two electrode setup, using Ti foil as working electrode and graphite rod as counter electrode.

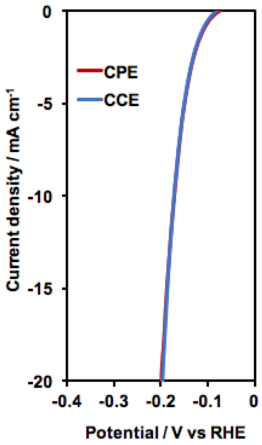


**Fig. S24** HER activity test of Ni-P film prepared under CPE (red) or CCE (blue). Polarization data were collected in 0.5 M $H_2SO_4$ at a scan rate of 3 mV/s.

### *18. Crystallographic Information*

Refinement Details—In each case, crystals were mounted on a glass fiber or MiTeGen loop using Paratone oil, then placed on the diffractometer under a nitrogen stream. Low temperature (100 K) X-ray data were obtained on a Bruker D8 VENTURE Kappa Duo PHOTON 100 CMOS based diffractometer (Mo $I_{\mu}S$ HB micro-focus sealed X-ray tube, $K_{\alpha} = 0.71073$ Å). All diffractometer manipulations, including data collection, integration, and scaling were carried out using the Bruker APEXIII software.[10] Absorption corrections were applied using SADABS.[11] Space groups were determined on the basis of systematic absences and intensity statistics and the structures were solved in the Olex 2 software interface[10-11] by intrinsic phasing using XT (incorporated into SHELXTL) and refined by full-matrix least squares on $F^2$. All non-hydrogen atoms were refined using anisotropic displacement parameters. Hydrogen atoms were placed in the idealized positions and refined using a riding model. The structures were refined (weighed least squares refinement on $F^2$) to convergence. Graphical representation of structures with 50% probability thermal ellipsoids were generated using Diamond 3 visualization software.[12]

**Table S1—**Crystal and refinement data for complexes **1-3**.

| | **1** | **2** | **3** |
|---|---|---|---|
| CCDC Number[13] | 1578146 | 1578147 | 1578145 |
| Empirical formula | $C_{40}H_{48}Cl_2N_2NiO_2P_2$ | $C_{40}H_{44}N_2NiP_2$ | $C_{152}H_{132}Cl_8Ni_2P_8$ |
| Formula weight | 780.35 | 673.42 | 2607.35 |
| T (K) | 100 | 100 | 100 |
| *a*, Å | 17.275(1) | 10.1578(5) | 15.3354(8) |
| *b*, Å | 11.6325(7) | 12.6891(7) | 26.211(2) |
| *c*, Å | 18.682(1) | 13.5459(7) | 16.442(1) |
| α, ° | 90 | 101.964(2) | 90 |
| β, ° | 90.593(2) | 90.747(2) | 103.332(2) |
| γ, ° | 90 | 105.179(2) | 90 |
| Volume, Å$^3$ | 3753.9(4) | 1644.27(15) | 6430.6(6) |
| Z | 4 | 2 | 2 |
| Crystal system | Monoclinic | Triclinic | Monoclinic |
| Space group | $P2_1/n$ | $P\bar{1}$ | $P2_1/n$ |
| $d_{calc}$, g/cm$^3$ | 1.381 | 1.360 | 1.347 |
| θ range, ° | 2.358 to 38.883 | 2.307 to 36.318 | 2.258 to 36.778 |
| $\mu$, mm$^{-1}$ | 0.782 | 0.720 | 0.612 |
| Abs. Correction | Semi-empirical | Semi-empirical | Semi-empirical |
| GOF | 1.046 | 1.030 | 1.043 |
| $R_1$ ,[a] $wR_2$ [b] [I>2 σ(I)] | 0.0318, 0.0754 | 0.0401, 0.0801 | 0.0571, 0.1283 |
| Diffractometer | PHOTON | PHOTON | PHOTON |
| Radiation Type | Mo $K_\alpha$ | Mo $K_\alpha$ | Mo $K_\alpha$ |

[a] $R_1 = \sum||F_o| - |F_c||/\sum|F_o|$. [b] $wR_2 = [\sum[w(F_o^2-F_c^2)^2]/\sum[w(F_o^2)^2]^{1/2}$

**Special refinement detail of 1:**

Disordered two THF solvent molecules were present in the crystal packing voids. The disorder was satisfactorily modeled with populations as follow: C33A/B through C36A/B and O1A/B 20:80 ratio, C37A/B through C40A/B and O2A/B 44:56 ratio.

**Special refinement detail of 3:**

Crystals of complex 3 were non-merohedrally twinned and satisfactorily modeled as a 0.63:0.37 ratio of two twin components.

## 19. Reference


[1] A. B. Pangborn, M. A. Giardello, R. H. Grubbs, R. K. Rosen, F. J. Timmers, *Organometallics* **1996**, *15*, 1518-1520.

[2] A. Velian, M. Nava, M. Temprado, Y. Zhou, R. W. Field, C. C. Cummins, *J. Am. Chem. Soc.* **2014**, *136*, 13586-13589.

[3] P. K. Freeman, L. L. Hutchinson, *J. Org. Chem.* **1983**, *48*, 879-881.

[4] A. B. Burg, P. J. Slota, *J. Am. Chem. Soc.* **1958**, *80*, 1107-1109.

[5] G. R. Fulmer, A. J. M. Miller, N. H. Sherden, H. E. Gottlieb, A. Nudelman, B. M. Stoltz, J. E. Bercaw, K. I. Goldberg, *Organometallics* **2010**, *29*, 2176-2179.

[6] a) S. Rundqvist, E. Hassler, L. Lundvik, K. Motzfeldt, O. Theander, H. Flood, *Acta Chem. Scand.* **1962**, *16*, 242-243. b) Chykhrij S.I., Kuz'ma Y.B., *Russ. J. Inorg. Chem.*, **1990**, *35*, 1821-1823.

[7] E. J. Popczun, J. R. McKone, C. G. Read, A. J. Biacchi, A. M. Wiltrout, N. S. Lewis, R. E. Schaak, *J. Am. Chem. Soc.* **2013**, *135*, 9267-9270.

[8] M. H. Tang, C. Hahn, A. J. Klobuchar, J. W. Ng, J. Wellendorff, T. Bligaard, T. F. Jaramillo, *Phys Chem Chem Phys* **2014**, *16*, 19250-19257.

[9] M. S. Faber, R. Dziedzic, M. A. Lukowski, N. S. Kaiser, Q. Ding, S. Jin, *J. Am. Chem. Soc.* **2014**, *136*, 10053-10061.

[10] Sheldrick, G.M. "SADABS (version 2008/2001): Program for Absorption Correction for Data from Area Detector Frames", University of Göttingen, 2008.

[11] O. V. Dolomanov, L. J. Bourhis, R. J. Gildea, J. A. K. Howard, H. Puschmann, *Journal of Applied Crystallography* **2009**, *42*, 339-341.

[12] Brandenburg, K. (1999). DIAMOND. Crystal Impact GbR, Bonn, Germany.

[13] Crystallographic data have been deposited at the CCDC, 12 Union Road, Cambridge CB12 11EZ, UK and copies can be otained on request, free of charge, by quoting the publication citation and the respective deposition numbers.